

Electron microscopic evidence for nucleation and growth of 3D acetylcholine receptor microcrystals in structured lipid–detergent matrices

Yoav Paas^{*†}, Jean Cartaud[‡], Michel Recouvreur[‡], Regis Grailhe^{*}, Virginie Dufresne^{*}, Eva Pebay-Peyroula[§], Ehud M. Landau[¶], and Jean-Pierre Changeux^{*†}

^{*}Récepteurs et Cognition, Unité de Recherche Associée 2182, Centre National de la Recherche Scientifique, Institut Pasteur, 25 Rue du Docteur Roux, 75724 Paris Cedex 15, France; [‡]Biologie Cellulaire des Membranes, Institut Jacques Monod, Unité Mixte de Recherche 7592, Centre National de la Recherche Scientifique, Universités Paris 6 et Paris 7, 75251 Paris, France; [§]Institut de Biologie Structurale, Commissariat à l'Énergie Atomique–Centre National de la Recherche Scientifique–Université Joseph Fourier Unité Mixte de Recherche 5075, 41 Rue Jules Horowitz, F-38027 Grenoble Cedex 1, France; and [¶]Membrane Protein Laboratory, Sealy Center for Structural Biology, and Department of Physiology and Biophysics, University of Texas Medical Branch, 301 University Boulevard, Galveston, TX 77555-0437

Contributed by Jean-Pierre Changeux, July 16, 2003

Nicotinic acetylcholine receptors (AChRs) belong to a superfamily of oligomeric proteins that transduce electric signals across the cell membrane on binding of neurotransmitters. These receptors harbor a large extracellular ligand-binding domain directly linked to an ion-conducting channel-forming domain that spans the cell membrane 20 times and considerably extends into the cytoplasm. Thus far, none of these receptor channels has been crystallized in three dimensions. The crystallization of the AChR from *Torpedo marmorata* electric organs is challenged here in lipidic–detergent matrices. Detergent-soluble AChR complexed with α -bungarotoxin (α BTx), a polypeptidic competitive antagonist, was purified. The AChR– α BTx complex was reconstituted in a lipidic matrix composed of monoolein bilayers that are structured in three dimensions. The α BTx was conjugated to a photo-stable fluorophore, enabling us to monitor the physical behavior of the receptor–toxin complex in the lipidic matrix under light stereomicroscope, and to freeze fracture regions containing the receptor–toxin complex for visualization under a transmission electron microscope. Conditions were established for forming 2D receptor–toxin lattices that are stacked in the third dimension. 3D AChR nanocrystals were thereby grown inside the highly viscous lipidic 3D matrix. Slow emulsification of the lipidic matrix converted these nanocrystals into 3D elongated thin crystal plates of micrometer size. The latter are stable in detergent-containing aqueous solutions and can currently be used for seeding and epitaxial growth, en route to crystals of appropriate dimensions for x-ray diffraction studies.

nicotinic acetylcholine receptor | crystallization | structure

To date, the crystal structures of ≈ 50 integral membrane proteins have been determined at atomic resolution. This result is in stark contrast to their abundance, as they comprise one-third of all gene products. Inherent difficulties with high-level expression, purification, and, particularly, crystallization of integral membrane proteins account for this situation (1). Receptor channels that selectively regulate transport of ions across the cell membrane are large membrane-spanning oligomers. Among them are the pentameric ligand-gated ion channels (also termed the Cys-loop receptors), which mediate and modulate fast cell–cell communication throughout the nervous system.

The first and most extensively studied pentameric ligand-gated ion channel is the acetylcholine receptor (AChR; reviewed in refs. 2–4). The AChR isolated from the electric organs of *Torpedo* ray is available in milligram amounts suitable for crystallization experiments. It is a pseudosymmetrical glycoprotein of ≈ 290 kDa comprised of five subunits ($2\alpha\beta\gamma\delta$) and carries two ACh-binding sites at the α – γ and α – δ boundaries (2, 3). So far, it was possible to organize this oligomeric protein only in tubular 2D crystals within receptor-rich membrane fragments (5,

6). These crystals enabled the collection of electron diffraction data at 9-Å down to 4-Å resolution (refs. 7 and 8 and references therein).

As with other pentameric ligand-gated ion channels, a few reasons account for the receptor's difficulty to form ordered 3D crystals that are necessary for x-ray structure determination at atomic resolution. First, it is a highly amphiphilic oligomer, characterized by a large hydrophobic region that consists of 20 transmembrane segments and two hydrophilic domains: (i) a ligand-binding domain that protrudes extracellularly by ≈ 8 nm and displays an 8- to 9-nm diameter (7) and (ii) an intracellular domain that protrudes by ≈ 4.5 nm into the cytoplasm and displays a diameter that narrows from ≈ 8 to ≈ 4 nm (7). Second, it is an allosteric protein that interconverts spontaneously between at least three alternative, discrete conformations: resting, active, and desensitized states (2, 3). Third, the receptor is glycosylated with high-mannose and complex oligosaccharides (9).

Here, we report the 3D crystallization of the *Torpedo* AChR by extending a methodology successfully used with several archaeal rhodopsins (10–15) which, unlike the AChR, are small proteins mostly embedded in the lipid bilayer.

Materials and Methods

Preparation of AChR– α -bungarotoxin (α BTx) Complexes for Crystallization. All purification steps were performed at 4°C and included, with one exception, protease inhibitor mixture (Sigma). Preparations of *Torpedo* AChR-rich membranes and removal, by alkaline treatment, of the 43-kDa rapsyn protein that is associated with the receptor, were performed basically as described (16). The alkaline-treated membranes (1 mg/ml) were then solubilized in buffer containing 5 mM Hepes, 80 mM NaCl, and 6.5 mM 3-[(3-cholamidopropyl)dimethylammonio]-1-propanesulfonate (CHAPS; pH 7.4). The CHAPS-soluble AChR was immobilized on affinity resin. The affinity resin was prepared by reacting Affi-Gel 102 (Bio-Rad) with *N*-acetyl-DL-homocysteine thiolactone (Sigma) to form sulfhydryl-terminal-crosslinked agarose (17), which then was reacted with bromo-acetylcholine bromide (18) as described (19).

After extensive wash of the AChR-bound resin with solubilization buffer, tetramethylrhodamine– α BTx conjugate (Molecular Probes; ≈ 2 -fold molar excess over α BTx-binding sites) was cycled slowly through the column until it diffused homoge-

Abbreviations: AChR, acetylcholine receptor; α BTx, α -bungarotoxin; CHAPS, 3-[(3-cholamidopropyl)dimethylammonio]-1-propanesulfonate; MO, monoolein; EM, electron microscopy.

[†]To whom correspondence should be addressed. E-mail: ypaas@pasteur.fr, ypaas@panor.co.il, or changeux@pasteur.fr.

© 2003 by The National Academy of Sciences of the USA

neously throughout the resin. After a further few hours of incubation, the mobile AChR- α BTx complexes and the free α BTx were collected and subjected to concentration by using centrifugal filter device with a 100-kDa nominal molecular mass limit (Amicon, Millipore). Removal of free α BTx was obtained after repetitive dilution/concentration steps, which were performed in the absence of protease inhibitors. Note that, throughout the purification process, the concentration of α BTx was systematically kept above 6 μ M. Finally the AChR- α BTx was concentrated to 20–25 mg/ml, and DTT was added to maximal 1 mM concentration to obtain homogenous light AChR form (monomeric pentamers) (20, 21). Notably, stopped-flow experiments indicate that CHAPS stabilizes the receptor population in a high-affinity desensitized state progressively with the increase in detergent:lipid ratio (data not shown and ref. 22). Conclusively, here, during unbinding and displacement of the resin-immobilized acetylcholine by the toxin, the receptor remains in its desensitized state. This conclusion is in line with previous studies that showed that α BTx or other α -toxins bind with a very high affinity (K_d in picomolar range) to AChR that is solubilized by, and kept in, desensitizing detergents (e.g., refs. 23 and 24 and references therein).

Crystallization. Purified AChR- α BTx complexes were incorporated with monoolein (monooleoyl-*rac*-glycerol [C18:1c9]; NU CHEK) as described (25) at receptor concentration of 8–10 mg/ml. The resulting lipidic phase was then overlaid with solutions of various chemical compositions. Birefringent red patches were obtained at 20°C with an overlaying solution containing 0.1 M sodium cacodylate, 18% wt/vol polyethylene glycol (PEG) 8000, 0.2 M calcium acetate, 0.5 mM DTT, and 0.02% sodium azide (pH 6.5–6.8). As soon as birefringence reached its maximum (usually within 2–6 wk, depending on the concentration of protein in the patch), the overlay solution was exchanged by liquefaction solution containing 0.1 M Hepes, 28% wt/vol PEG 400, 0.2 M calcium chloride, 3.5–6.5 mM CHAPS, 0.5 mM DTT, and 0.02% sodium azide (pH 7.2). The samples were occasionally transferred to 27–30°C and inspected routinely under a light microscope. With time, the highly viscous and transparent cubic phase became turbid and then turned into an emulsion containing red micrometer-sized crystals. The latter were harvested with nylon loops, soaked in liquefaction solution supplemented with 30% (wt/wt) glycerol, and cryo-cooled rapidly to \approx 100 K in liquid propane. Crystals were examined for diffraction at beam line ID14 of the European Synchrotron Radiation Facility (ESRF), Grenoble, France.

Electron Microscopy (EM). For EM studies, the entire lipidic phase was removed from the tube with a fine spatula, and the red birefringent patches were separated from the bulk lipidic matrix by using microtools. A decrease in birefringence that reflects loss of crystallinity was observed during these mechanical manipulations. The resulting material was gently compressed and flattened between two copper-made specimen holders (Bal-Tec, Liechtenstein), cryo-cooled in liquid propane and quickly transferred to liquid nitrogen. Specimens were fractured at -150°C , shadowed with platinum, and coated with carbon in a Balzers 310 apparatus (Balzers), all under high vacuum conditions as described (26) but with no prefixation of the red birefringent material. The resulting replicas were cleaned, placed on collodion-coated EM grids, and inspected in a CM 12 electron microscope (Philips, The Netherlands) operating at 80 keV. Micrographs were taken on Kodak Electron Image plates.

Results

Purification of AChR- α BTx Complexes for Crystallization. The crystallization experiments presented here use AChR molecules associated with tetramethylrhodamine- α BTx conjugates. α BTx is a highly specific competitive antagonist of the *Torpedo* AChR

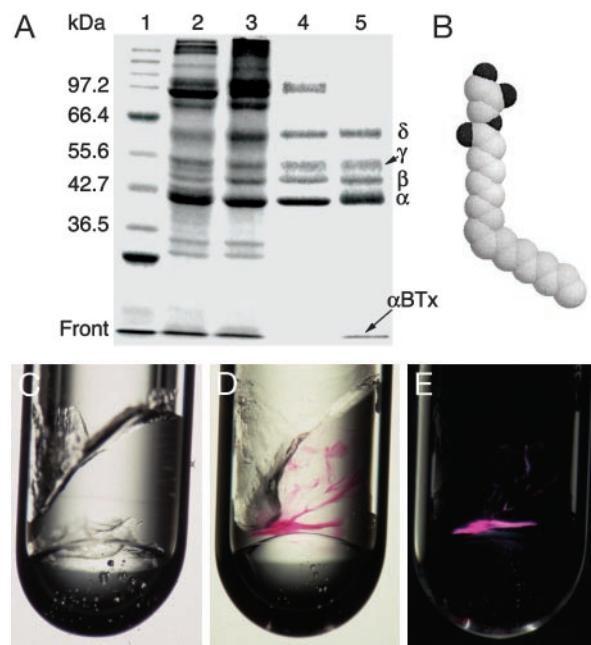


Fig. 1. Incorporation of AChR- α BTx complexes into a lipidic 3D matrix. (A) Reducing SDS-polyacrylamide gel (9%) showing the purification steps: lane 1, molecular mass markers; lane 2, receptor-rich membranes; lane 3, pH 11-treated receptor-enriched membranes; lane 4, CHAPS-solubilized receptor; lane 5, purified fraction. α BTx (8.5 kDa) that migrates at the front and the receptor subunits are indicated. Shown is a gel stained by Coomassie brilliant blue. (B) Space-filling model of a MO molecule. Dark and light spheres correspond to oxygen and carbon atoms, respectively. (C) MO mixed with the protein-carrier buffer at MO:buffer ratio of 6:4 (wt/wt). The inner diameter of the glass tube is 2.5 mm. (D) Example of purified AChR- α BTx complexes concentrated inside the lipidic phase; the red color corresponds to tetramethylrhodamine that is covalently attached to the toxin. Shown is a picture taken under regular light. (E) The same sample as shown in D but under polarized light. Note that only regions that contain receptor-toxin complexes become birefringent. Also, there are regions that are red but not birefringent; their portion may vary between \approx 5% and 40% of the total incorporated AChR- α BTx.

(27). Like other α -neurotoxins (28–32), α BTx binds to skeletal muscle AChRs, blocking thereby the postsynaptic activity in the neuromuscular junction. Two α BTx molecules can specifically bind one receptor heteropentamer. The affinity of the toxin for both sites of a detergent-soluble *Torpedo* AChR is similar and very high (23), displaying equilibrium dissociation constant (K_d) in the picomolar range. The half-life of the complex is >10 days (23). Accordingly, no detachment of the toxin from the receptor was observed during the preparation of AChR- α BTx complexes. Lane 5 of Fig. 1A shows the bands corresponding to the *Torpedo* receptor subunits and the rhodaminylated α BTx. We refer to this detergent-soluble purified complex as a desensitized, α BTx-bound stable receptor (see *Materials and Methods*).

Incorporation of AChR- α BTx Complexes in a Bilayer-Based 3D Matrix. Monoolein (MO) is a lipid whose small, uncharged hydrophilic glycerol head is linked to an 18-carbon-long alkenyl chain via an ester bond (Fig. 1B). A cis-double bond between C9 and C10 confers to the alkenyl chain a kink, which contributes to the wedge shape of this lipid. Fig. 1C shows the lipidic phase formed on mixing MO with a buffer devoid of protein. This phase is highly viscous, isotropic, transparent, and nonbirefringent, indicative of a cubic phase that consists of curved bilayers organized in three dimensions (refs. 25 and 33; see ref. 34 for a schematic representation).

Fig. 1D shows AChR- α BTx complexes incorporated and con-

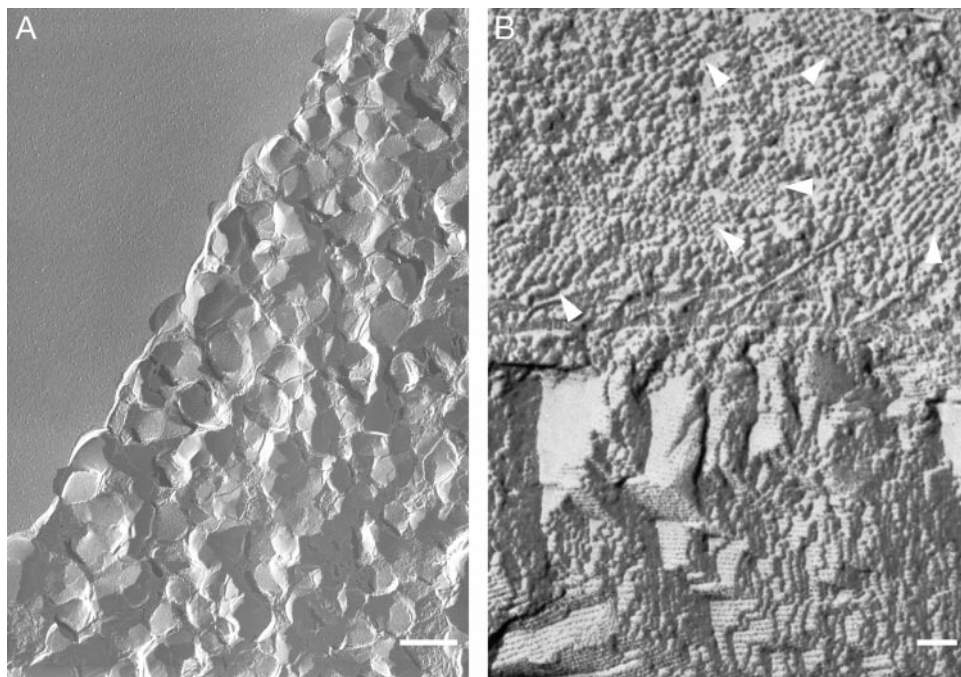


Fig. 2. Transmission electron micrographs of regions containing AChR- α BTx complexes. (A) Freeze fracture of red-labeled birefringent regions such as those shown in Fig. 1 *D* and *E* reveals many nanocrystals. Note that the upper left corner corresponds to a flat lipidic surface devoid of nanocrystals. (Scale bar = 0.5 μ m.) (B) Top view of a freeze-fracture plane showing segregation between particle-containing (upper part) and particle-devoid (lower part) regions. The arrows indicate six of numerous small regions consisting of spherical particles that are densely packed as highly ordered aggregates reminiscent of nuclei and tiny nanocrystals. The terrace-like architecture depicted in the lower part corresponds to \approx 4-nm-width layers stacked on top of each other. (Scale bar = 50 nm.) The white/grayish areas are shadowed by platinum.

centrated inside the MO cubic phase. The red color corresponds to tetramethylrhodamine that is covalently attached to α BTx. Tetramethylrhodamine is a photostable fluorophore that absorbs at 555-nm and emits at 580-nm wavelengths. Hence, the physical appearance of, and changes in, the AChR- α BTx complexes inside the lipidic cubic phase could be monitored by using a light stereomicroscope. Numerous conditions for crystallization were tested by overlaying the cubic phase with solutions of various chemical compositions. Because the aqueous compartments of the cubic phase are sufficiently large to accommodate hydrophilic molecules as large as lysozyme (35), small solutes could penetrate into the cubic phase and interact with the hydrophilic portions of the incorporated receptor-toxin complexes. Under most conditions screened for crystallization, no diffusion of red material from the viscous lipidic phase to the overlaying phase was observed, indicating a stable receptor-toxin complex.

Specific crystallization conditions rendered the red patches birefringent, as visualized under cross polarizers (Fig. 1*E*). This finding indicates polycrystallinity (36) and formation of intermolecular contacts.

EM Reveals Dense 2D AChR Lattices That Are Stacked in the Third Dimension. To directly visualize the organization of AChR- α BTx complexes in the lipidic phase, the red-labeled patches were inspected under electron microscope (see *Materials and Methods*). Fig. 2*A* shows a region containing nanometer-sized polygonal bodies reminiscent of nanocrystals. Some of these bodies are embedded in the lipidic matrix and protrude toward the viewer whereas others detached probably owing to the fracturing action, leaving behind depressions with a print of their shape.

Fig. 2*B* shows a more detailed fracture plane that exhibits segregation between two types of architectures. The upper part depicts densely packed, spherical particles of an \approx 8- to 9-nm

diameter. This diameter is in accord with the size previously shown for the AChR in membranes prepared from the *Torpedo* electric organs (ref. 7 and references therein, and ref. 26). Some small regions displaying highly ordered aggregates could clearly be seen (Fig. 2*B*, upper part). The lower part does not contain any particles as it reflects lamellar-crystalline organization (34), characterized by lipidic lamellae stacked on top of each other, with no sufficient water in between to accommodate the hydrophilic portions of the receptor.

Freeze-fracture through rhodamine-labeled birefringent material also revealed numerous highly dense 2D lattices of spherical particles (e.g., Fig. 3). As before, the diameter of the particles fits with the molecular size of the *Torpedo* AChR. Despite the low resolution of the EM technique used here, the pit of the receptor could readily be identified as a black spot surrounded by the receptor subunits (Fig. 3), giving rise to the doughnut-like shape typical of the AChR (5-7, 26). Careful inspection of the transmission EM micrographs indicates defects in these lattices: for instance, collapse of receptor particles (e.g., Fig. 3*A*), dislocations (e.g., Fig. 3*B*), and cracks that could readily be distinguished from regular facets (e.g., Fig. 3*C*).

Fracturing perpendicularly to the planes shown in Fig. 3 exposed highly dense layers that are stacked on each other (e.g., Fig. 4*A*). Despite the heavy damages seen in this fracture plane, single AChR molecules that were split along their longitudinal axis were visualized (Fig. 4*B*). These molecules display the shape and dimensions typical of the receptor in tubular 2D crystals (37) (Fig. 4, compare *B* to *C*). The receptor molecules are packed tail to tail (Fig. 4*B*) and probably interact via their heads to form the multilayer architecture seen in Fig. 4*A*, as illustrated in Fig. 4*D*.

Emulsification of the Lipidic Matrix Triggers the Formation of AChR Microcrystals. To obtain crystals that are larger than those shown in Figs. 2*A* and 3, the hydration level of the cubic phase was

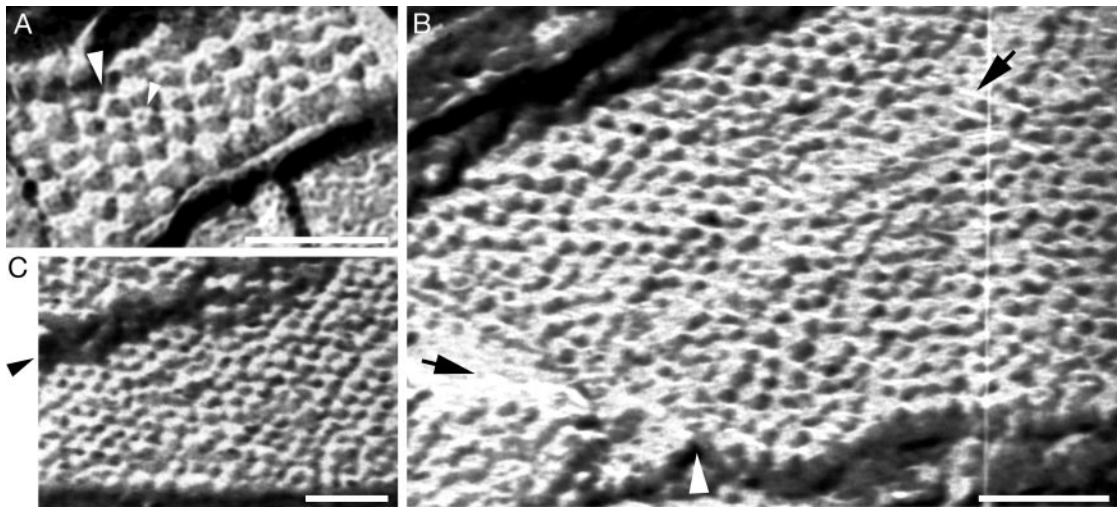


Fig. 3. AChR- α BTx complexes are organized in 2D lattices. (A) Top view of a nanometer-sized crystal reflecting nucleation of receptor-toxin complexes inside the MO cubic phase. The small arrow indicates a receptor molecule that appears like a doughnut displaying five subunits surrounding a black pit. The diameter of this receptor is ≈ 9 nm. The large arrow indicates a receptor molecule that collapsed and coalesced with the neighboring right-handed receptor. (B) Top view of a region showing hundreds of spherical particles organized side by side in linear rows. These particles correspond to AChR molecules, as discussed in the text. The black arrow in the upper right corner points to a defect propagating along the nanocrystal. The black and white arrows at the bottom left corner point to a contact area between two nanocrystals. Regular facets can be seen at the upper and lower edges. (C) A wide crack along a nanocrystal is pointed by the arrow. A regular facet can be visualized at the lower edge. In all panels, the scale bars correspond to 50 nm, and the white/grayish areas are shadowed by platinum.

increased and detergents were used to perturb its highly viscous consistency. Elongated thin crystal plates appeared in the resulting emulsion. Such reproducible crystals (e.g., Fig. 5A) are

homogeneously red and display clear facets. Stronger color is observed for the larger crystals, which consist of a larger number of AChR- α BTx complexes. These crystals appear birefringent

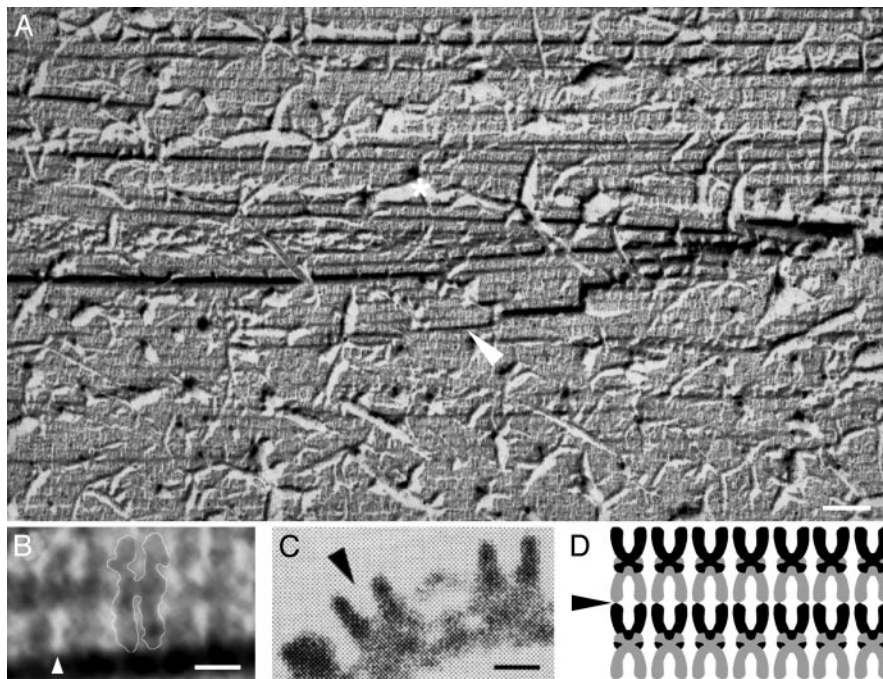


Fig. 4. AChR- α BTx complexes are organized in layers stacked in the third dimension. (A) Freeze-fracture plane passing through a mid-longitudinal axis of the receptor molecules exposes a multilayer organization. The grayish ruptures (one is indicated by a white asterisk) correspond to pieces that were torn apart from the fracture plane. The region indicated by the white arrow is magnified in B. Note that many receptor molecules collapsed, probably because of the fracturing through hard proteinaceous material. The receptor molecules are darkened, and the pits are white/grayish. (Scale bar = 50 nm.) (B) Magnification of six "U-shaped" constituents of the region indicated in A by a white arrow. These receptor molecules are arranged side by side and are tightly packed tail to tail. For convenience, a white line delineates the boundaries of the middle receptor dimer. The white arrow indicates the pit of a receptor molecule as can be compared with the pit shown in C. (Scale bar = 50 Å.) (C) Side view of AChR molecules as seen in a portion of a tubular 2D crystal previously obtained from pH 11-treated membranes. [Reproduced with permission from ref. 37 (Copyright 1988, Nature Publishing Group, www.nature.com).] The arrow points to the receptor's pit. (Scale bar = 50 Å.) (D) Scheme illustrating the packing pattern of the receptor molecules as concluded from A and B. The arrow indicates an initiation point for a fracture that would provide a top view of the lattice, as observed in many fracture planes (e.g., Fig. 3).

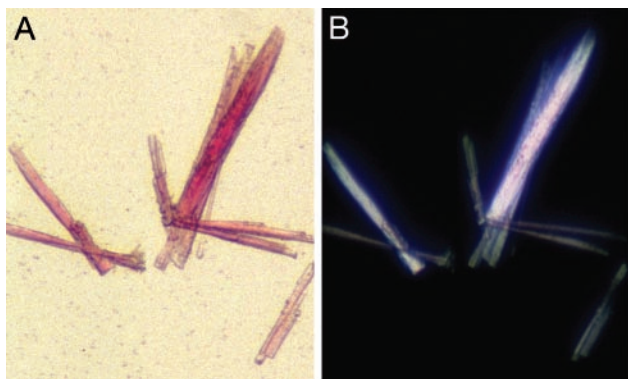


Fig. 5. Emulsification of the lipidic phase results in growth of micrometer-sized AChR- α BTx crystals. (A) A few thin crystal plates that grew on slow liquefaction of MO cubic phase that harbored AChR- α BTx nanocrystals. Shown is a picture taken under a regular light. The dimensions of the largest crystal are: $300\ \mu\text{m} \times 30\ \mu\text{m} \times \approx 15\ \mu\text{m}$. (B) The same crystals as shown in A but under polarized light.

under crossed polarizers (Fig. 5B), indicating some high degree of order.

Note that, in a separate set of experiments (performed as in ref. 23), no detachment of [^{125}I] α BTx from preformed AChR-[^{125}I] α BTx complexes was detected under the crystallization and emulsification conditions.

Discussion

Reconstitution of the *Torpedo* AChR in MO-based 3D matrix allowed here the nucleation and crystallization of a glycosylated full-length receptor channel in three dimensions. Depending on hydration, temperature, and pressure, MO can form a variety of mesophases, including the lamellar, cubic, and inverted hexagonal phases (33, 34). In the cubic phase, the MO bilayers are isotropically curved in 3D space, and they separate between two channel-like aqueous compartments. A reconstituted membrane protein can diffuse laterally in the three dimensions of the cubic phase, provided that the aqueous compartments of the cubic phase are sufficiently large to accommodate the extra-membranous portions of the incorporated protein (10, 38). Yet, rotational and translational constraints that are dictated by the cubic phase architecture lead to ordered nucleation and crystallization, possibly as proposed for bacteriorhodopsin (34, 39).

The diameter of the water channels in pure MO-water cubic phase at room temperature is $\approx 50\ \text{\AA}$. Thus, a major question in the current study is how the *Torpedo* AChR, which harbors an extracellular domain $\approx 80\text{--}90\ \text{\AA}$ in diameter and protrudes from the lipid bilayer by $\approx 80\ \text{\AA}$, can be incorporated in such a lipidic cubic phase. Moreover, the diameter of the AChR- α BTx complex would be even larger because α -toxins probably dock at the exterior wall of AChRs, as predicted by computational models (40–43) that became feasible only after the x-ray structure of a water-soluble ACh-binding protein (44) was determined at atomic resolution (45). To accommodate such a large domain, either the cubic phase has to undergo a local structural change, or it may undergo a phase transition and adopt a noncubic structure. One can therefore anticipate that the lamellar liquid-crystalline phase may constitute a favorable lipidic environment for AChR- α BTx complexes. This phase (see a scheme in ref. 34) consists of planar bilayer sheets stacked in the third dimension and spaced by aqueous compartments with repeat distance that depends on various parameters like hydration, polarity of the lipid head groups, and ionic strength. A spacing distance sufficient for nesting the large hydrophilic extra-membranous domains of the receptor would allow incorporation of the receptor in the lamellar liquid-crystalline phase. The size of the extra-membranous domains and the manner

by which receptors in one sheet interact with receptors in the flanking sheets would ultimately determine the spacing distance between the receptor-containing sheets, leading thereby to a multilayer organization with a specific packing pattern.

By using light microscopy and EM, the conditions necessary for reconstituting AChR- α BTx complexes in MO 3D-matrix, while maintaining the toxin associated to the receptor, were established. The appearance of birefringent polycrystalline aggregates (Fig. 1D and E) reflects the nucleation and growth of nanocrystals (Figs. 2 and 3). The spherical particles that compose these nanocrystals correspond to AChR- α BTx complexes seen from a top view, as (i) only purified AChR- α BTx complexes were used in the reconstitution step; (ii) these complexes were stably labeled with rhodamine, a fluorophore covalently attached to α BTx; and (iii) these particles display the shape and dimensions typical of the AChR, as previously visualized in native membrane preparations (5–7, 26). Moreover, despite the low resolution of the applied freeze fracture/transmission EM techniques, the pit surrounded by the walls of the receptor's extracellular domain was, in most cases, readily identified (e.g., Fig. 3A and B). Fracture planes that correspond to receptor mid-sagittal sections revealed multilayer organization of receptor molecules that are packed tail to tail as dimers (e.g., Fig. 4A and B). The two heads of each dimer interact with the heads of two different dimers from the flanking layers, as schematically illustrated in Fig. 4D.

The low-resolution EM technique used here does not allow us to conclude on the lateral complex–complex interactions. In the case of ACh-binding protein, lateral interactions play a role in crystal packing (45), leaving no space to accommodate α BTx by the crystallized form (PDB ID number 119B, see crystallographic symmetry). Here, it seems that there is some separation between particles (Figs. 3 and 4). Hence, crystallization of a preformed receptor–toxin complex with a different pattern of lateral interactions cannot be excluded.

As pointed out above, the fracture planes exhibit defects such as collapse of receptor particles and cracks in nanocrystals (e.g., Figs. 3 and 4). It is reasonable to assume that these defects occurred after the nanocrystals grew, due to mechanical damage taking place either when preparing the specimens for EM studies (see *Material and Methods*) or while fracturing through the hard proteinaceous material. We do not, however, exclude defects, such as dislocations, that might take place already during the growth of nanocrystals in the lipidic 3D matrix.

Taken together, these results demonstrate that the birefringent red material grown in the lipidic matrix consists of nanometer-sized 3D crystals of AChR- α BTx complexes. As these nanocrystals touch each other (Fig. 2A), the growth of larger crystals is inhibited.

Notably, part of the rhodamine-labeled material does not exhibit birefringence (Fig. 1D and E). These regions probably correspond to disordered aggregates visualized by transmission EM (data not shown). By emulsifying the lipidic matrix, we aimed at releasing single AChR- α BTx complexes from the disordered aggregates, thereby allowing them to attach to the surface of nanocrystals that detach from each other. Attachment of single molecules to a surface of a preexisting crystal is a fundamental process in crystallization of macromolecules (46). Indeed, micrometer-sized crystals appear in the emulsion. As reported in *Results*, the crystallization and emulsification conditions did not lead to detachment of the toxin from the receptor. Hence, as can be judged from their optical properties, these microcrystals are comprised of AChR- α BTx complexes; they display a homogeneous red color and, as expected, larger crystals display stronger red color because they contain more labeled complexes. These crystals exhibit clear facets, and they are birefringent, indicating a high degree of order.

Thus far, these reproducible crystals did not diffract x-rays, probably because they are too thin and perhaps not perfectly ordered. Nevertheless, they can readily be removed and stabilized outside the emulsion for further manipulations. Using these microcrystals as a source of preexisting crystalline surfaces (seeds) would allow decreasing the high degree of supersaturation and energy that are necessary for nucleation in aqueous (detergent) solutions (36). Thus, in a second step of crystallization, seeds prepared from these crystals will be used to trigger epitaxial growth of well-diffracting crystals directly from detergent-containing solutions, avoiding thereby the massive nucleation and precipitation that usually prevent efficient crystallization.

Finally, the ability to follow the development of nanocrystals in the MO 3D matrix, owing to their birefringent properties, and the capability to further develop them into micrometer-sized crystals, may allow the use of unlabeled protein. This procedure should pave the way for crystallization of other membrane-spanning proteins that resist crystallization.

Y.P. thanks the Human Frontier Science Program Organization, the Federation of European Biochemical Societies, and the Manlio Cantarini Foundation for postdoctoral fellowships, and Mr. I. Paas for considerable private support. This work was supported by the Collège de France, the Centre National de la Recherche Scientifique, the Association pour la Recherche contre le Cancer, and European Economic Community contracts.

- Rosenbusch, J. P. (2001) *J. Struct. Biol.* **136**, 144–157.
- Corringer, P. J., Le Novère, N. & Changeux, J. P. (2000) *Annu. Rev. Pharmacol. Toxicol.* **40**, 431–458.
- Karlin, A. (2002) *Nat. Rev. Neurosci.* **3**, 102–114.
- Engel, A. G., Ohno, K. & Sine, S. M. (2003) *Nat. Rev. Neurosci.* **4**, 339–352.
- Kistler, J. & Stroud, R. M. (1981) *Proc. Natl. Acad. Sci. USA* **78**, 3678–3682.
- Brisson, A. & Unwin, P. N. (1984) *J. Cell Biol.* **99**, 1202–1211.
- Unwin, N. (2000) *Philos. Trans. R. Soc. London B* **355**, 1813–1829.
- Miyazawa, A., Fujiyoshi, Y. & Unwin, N. (2003) *Nature* **423**, 949–955.
- Poulter, L., Earnest, J. P., Stroud, R. M. & Burlingame, A. L. (1989) *Proc. Natl. Acad. Sci. USA* **86**, 6645–6649.
- Landau, E. M. & Rosenbusch, J. P. (1996) *Proc. Natl. Acad. Sci. USA* **93**, 14532–14535.
- Pebay-Peyroula, E., Rummel, G., Rosenbusch, J. P. & Landau, E. M. (1997) *Science* **277**, 1676–1681.
- Luecke, H., Schobert, B., Richter, H. T., Cartailier, J. P. & Lanyi, J. K. (1999) *Science* **286**, 255–261.
- Kolbe, M., Besir, H., Essen, L. O. & Oesterhelt, D. (2000) *Science* **288**, 1390–1396.
- Luecke, H., Schobert, B., Lanyi, J. K., Spudich, E. N. & Spudich, J. L. (2001) *Science* **293**, 1499–1503.
- Royant, A., Nollert, P., Edman, K., Neutze, R., Landau, E. M., Pebay-Peyroula, E. & Navarro, J. (2001) *Proc. Natl. Acad. Sci. USA* **98**, 10131–10136.
- Neubig, R. R., Krodell, E. K., Boyd, N. D. & Cohen, J. B. (1979) *Proc. Natl. Acad. Sci. USA* **76**, 690–694.
- Karlin, A. & Cowburn, D. (1973) *Proc. Natl. Acad. Sci. USA* **70**, 3636–3640.
- Damle, V. N., McLaughlin, M. & Karlin, A. (1978) *Biochem. Biophys. Res. Commun.* **84**, 845–851.
- Reynolds, J. A. & Karlin, A. (1978) *Biochemistry* **17**, 2035–2038.
- Chang, H. W. & Bock, E. (1977) *Biochemistry* **16**, 4513–4520.
- Hamilton, S. L., McLaughlin, M. & Karlin, A. (1977) *Biochem. Biophys. Res. Commun.* **79**, 692–699.
- Martinez, K., Gohon, Y., Corringer, P., Tribet, C., Merola, F., Changeux, J. & Popot, J. (2002) *FEBS Lett.* **528**, 251–256.
- Conti-Tronconi, B. M., Tang, F., Walgrave, S. & Gallagher, W. (1990) *Biochemistry* **29**, 1046–1054.
- McCarthy, M. P. & Moore, M. A. (1992) *J. Biol. Chem.* **267**, 7655–7663.
- Rummel, G., Hardmeyer, A., Widmer, C., Chiu, M. L., Nollert, P., Locher, K. P., Pedruzzi, I. I., Landau, E. M. & Rosenbusch, J. P. (1998) *J. Struct. Biol.* **121**, 82–91.
- Cartaud, J., Benedetti, E. L., Sobel, A. & Changeux, J. P. (1978) *J. Cell Sci.* **29**, 313–337.
- Changeux, J. P., Kasai, M. & Lee, C. Y. (1970) *Proc. Natl. Acad. Sci. USA* **67**, 1241–1247.
- Lester, H. A. (1970) *Nature* **227**, 727–728.
- Lester, H. A. (1972) *Mol. Pharmacol.* **8**, 623–631.
- Meunier, J. C., Olsen, R. W., Menez, A., Fromageot, P., Boquet, P. & Changeux, J. P. (1972) *Biochemistry* **11**, 1200–1210.
- Prives, J. M., Reiter, M. J., Cowburn, D. A. & Karlin, A. (1972) *Mol. Pharmacol.* **8**, 786–789.
- Taylor, P., Osaka, H., Molles, B. E., Sugiyama, N., Marchot, P., Ackermann, E. J., Malany, S., McArdle, J. J., Sine, S. M. & Tsigelny, I. (1998) *J. Physiol. (Paris)* **92**, 79–83.
- Luzzati, V. (1997) *Curr. Opin. Struct. Biol.* **7**, 661–668.
- Caffrey, M. (2003) *J. Struct. Biol.* **142**, 108–132.
- Landau, E. M., Rummel, G., Cowan-Jacob, S. W. & Rosenbusch, J. P. (1997) *J. Phys. Chem. B* **101**, 1935–1937.
- Ducruix, A. & Giege, R. (1992) *Crystallization of Nucleic Acid and Protein: A Practical Approach* (Oxford Univ. Press, Oxford).
- Toyoshima, C. & Unwin, N. (1988) *Nature* **336**, 247–250.
- Gouaux, E. (1998) *Structure* **6**, 5–10.
- Nollert, P., Qiu, H., Caffrey, M., Rosenbusch, J. P. & Landau, E. M. (2001) *FEBS Lett.* **504**, 179–186.
- Harel, M., Kasher, R., Nicolas, A., Guss, J. M., Balass, M., Fridkin, M., Smit, A. B., Brejc, K., Sixma, T. K., Katchalski-Katzir, E., *et al.* (2001) *Neuron* **32**, 265–275.
- Fruchart-Gaillard, C., Gilquin, B., Antil-Delbeke, S., Le Novère, N., Tamiya, T., Corringer, P. J., Changeux, J. P., Menez, A. & Servent, D. (2002) *Proc. Natl. Acad. Sci. USA* **99**, 3216–3221.
- Moise, L., Piserchio, A., Basus, V. J. & Hawrot, E. (2002) *J. Biol. Chem.* **277**, 12406–12417.
- Samson, A. O., Scherf, T., Eisenstein, M., Chill, J. H. & Anglister, J. (2002) *Neuron* **35**, 319–332.
- Smit, A. B., Syed, N. I., Schaap, D., van Minnen, J., Klumperman, J., Kits, K. S., Lodder, H., van der Schors, R. C., van Elk, R., Sorgedraeger, B., *et al.* (2001) *Nature* **411**, 261–268.
- Brejck, K., van Dijk, W. J., Klaassen, R. V., Schuurmans, M., van Der Oost, J., Smit, A. B. & Sixma, T. K. (2001) *Nature* **411**, 269–276.
- Yau, S. T. & Vekilov, P. G. (2000) *Nature* **406**, 494–497.